Eur. Phys. J. D **17**, 181–188 (2001)

THE EUROPEAN PHYSICAL JOURNAL D

EDP Sciences

Measurement of the rotational alignment in the presence of the second order AC Stark effect

D. Wetzig, A.D. Rudert, and H. Zacharias[a]

Physikalisches Institut, Westfälische Wilhelms-Universität Münster, Wilhelm-Klemm-Straße 10, 48149 Münster, Germany

Received 1st August 2000 and Received in final form 2 May 2001

Abstract. The determination of the rotational quadrupole alignment of diatomic molecules *via* REMPI detection is investigated. In this process a high focal intensity usually increases the detection probability. At high intensities the AC Stark effect may cause a splitting of the normally degenerate m_J sublevels of a rotational state J beyond the spectral width of the exciting radiation. This leads to a selective detection of only certain m_J states with the consequence that deduced alignment factors can be misleading. From the theoretical considerations line profiles are explicitly calculated for dynamic polarizabilities which represent the $B\,^1\Sigma_u^+ \leftarrow X\,^1\Sigma_g^+$ transition of H_2, in order to fit an experimental (3+1) REMPI spectrum and to predict (1+1′) line shapes as a function of laser intensity. It is further shown that the deduced quadrupole alignment factor $A_0^{(2)}$ is significantly changed by the second order AC Stark effect when the intensities are chosen high enough to observe asymmetric broadened line profiles. Different combinations of relative linear polarizations of the exciting and ionizing laser beams are discussed.

PACS. 42.62.Fi Laser spectroscopy – 33.55.Be Zeeman and Stark effects – 33.15.-e Properties of molecules

1 Introduction

Since the pioneering theoretical work of Greene and Zare [1] the application of optical methods for the determination of the spatial alignment of molecules is finding an increasing acceptance. In combination with tunable laser excitation this method is increasingly applied for detecting molecular products of non-reactive [2–4] or reactive gas phase and surface collision [5–8]. Often resonantly enhanced multiphoton ionization (REMPI) employing pulsed laser radiation is used for the sensitive detection of such reaction products. In this case the sensitivity significantly increases with the exciting laser intensity. In these experiments the laser intensities either of the exciting or of the ionizing radiation usually exceed values of the order of a GW/cm^2. At such intensities the AC Stark effect and the resulting energetic splitting of the magnetic substates m_J of a rotational level J can no longer be neglected. Depending on the magnitude of this m_J state splitting compared to the spectral width of the exciting tunable laser radiation it may occur that only a subset of the m_J states can be observed by the optical transition. The determination of a spatial alignment of the molecules under investigation then becomes a difficult task.

The spectral line broadening in molecules at high laser intensities has been observed and first quantitatively analyzed by considering the AC Stark effect in two-photon excitation of CO [9] and NO [10]. Saturation effects in single photon excitation or in (1+1) REMPI due to high laser intensities at the resonant transition have been discussed by Jacobs and Zare [11]. This effect has not only properly to be taken into account when deducing the rovibrational state population of the initial state. Additionally, it may also have a marked influence on alignment parameters determined from varying the polarization of the exciting radiation. Polarization dependencies of the AC Stark effect on line broadening and splitting have more recently been discussed for multiphoton excitation and ionization of CO and N_2 [12]. In an earlier paper we have shown that the AC Stark effect can be exploited to prepare molecules spatially oriented to a significantly higher degree than at low intensities [13]. In the present paper we discuss the influence of the second order Stark effect on line profiles and the deduced quadrupole alignment factor $A_0^{(2)}$. For weak excitation and strong ionization laser fields the influence of the AC Stark effect on the deduced quadrupole alignment is shown in (1+1′) REMPI for various combinations of the laser polarizations. Examples are discussed for isotropic, helicoptering and cartwheeling molecules. The theoretical considerations are applied to calculate line profiles in (3+1) and (1+1′) REMPI of H_2 *via* the $B\,^1\Sigma_u^+ \leftarrow X\,^1\Sigma_g^+$ Lyman band.

In order to clearly show the influence of the AC Stark effect we restrict the discussion to the most simplest case of a $^1\Sigma$–$^1\Sigma$ transition performed by linearly polarized light. The strict ($\Delta m_J = 0$) selection rule prevents coherent couplings between magnetic substates. Coherence effects which may occur in more general cases, where intermediate states are produced by photodissociation [14] or where strong fields are resonantly coupled to the intermediate level [15–17] are not considered.

[a] e-mail: hzach@nwz.uni-muenster.de

2 The quadratic Stark effect

In a magnetic or electric field m_J states of the total angular momentum J, normally energetic degenerate, split in $(2J+1)$ (magnetic field) or $(J+1)$ (electric field) different levels. The magnitude of the splitting depends on the strength of the fields and the specific Hunds coupling cases between the different angular momenta in the molecule. In general, an electric field induces a decoupling of the spin Σ, the electronic angular momentum Λ and the pure rotational angular momentum N of the molecule. In the present work we discuss the electronic ${}^1\Sigma \leftarrow {}^1\Sigma$ transition of linear molecules. The electronic angular momentum Λ and the total spin Σ of the molecule are thus zero, and only the rotational motion contributes to the total angular momentum, if the nuclear spin is neglected.

In nonpolar molecules an external electric field $\mathbf{E}$ induces a polarization $\mathbf{P}$ in the electron cloud of the molecules. The induced polarization interacts with the external electric field resulting in an energetic splitting of the normally degenerate m_J sublevels. The interaction Hamiltonian $H_{\rm int}$ consists of the square of the electric field $\mathbf{E}$ and the polarizability $\boldsymbol{\alpha}$

$$H_{\rm int} = -\frac{1}{2}\sum_{i,j} E_i \alpha_{ij} E_j. \qquad (1)$$

For linear symmetric molecules in a ${}^1\Sigma$ state the evaluation of the matrix elements of the interaction Hamiltonian yields for a given angular momentum J [18,19]

$$\langle J, m_J \,|\mathbf{E}\,\boldsymbol{\alpha}\,\mathbf{E}|\, J, m_J\rangle = E^2\left[\frac{1}{3}\left(\alpha_\parallel + 2\alpha_\perp\right) - \frac{2}{3}\left(\alpha_\parallel - \alpha_\perp\right)\frac{3m_J^2 - J(J+1)}{(2J+3)(2J-1)}\right]. \qquad (2)$$

Here $\alpha_\parallel$ and $\alpha_\perp$ denote the components of the polarizability tensor parallel and perpendicular to the molecular symmetry axis, respectively. At a given laser intensity $I = c\epsilon_0 E^2/2$ an energetic splitting of each rotational level J into $|m_J|$ sublevels occurs. This energetic splitting is proportional to the anisotropic dynamic polarizability $\gamma = \alpha_\parallel - \alpha_\perp$, whereas the average dynamic polarizability $\alpha = (\alpha_\parallel + 2\alpha_\perp)/3$ accounts only for a general AC Stark shift of all levels.

In general, both the isotropic and the anisotropic polarizabilities depend on the frequency ω of the applied laser field and on the internuclear distance R at which the molecule is excited. In addition, electronic ground and excited states have to be considered separately. For the $\mathrm{B}\,{}^1\Sigma_u^+$ state of hydrogen Rychlewski *et al.* [20] have published results of theoretical calculations of the dynamic polarizabilities $\alpha_\parallel$ and $\alpha_\perp$. These values strongly depend on ω and R. For a particular vibronic intermediate state the effective polarizabilities $\alpha_\parallel$ and $\alpha_\perp$ can be obtained by averaging over the vibronic wavefunction:

$$\alpha_v(\omega) = \int \chi_v(R)\alpha(\omega, R)\chi_v(R)\,\mathrm{d}R. \qquad (3)$$

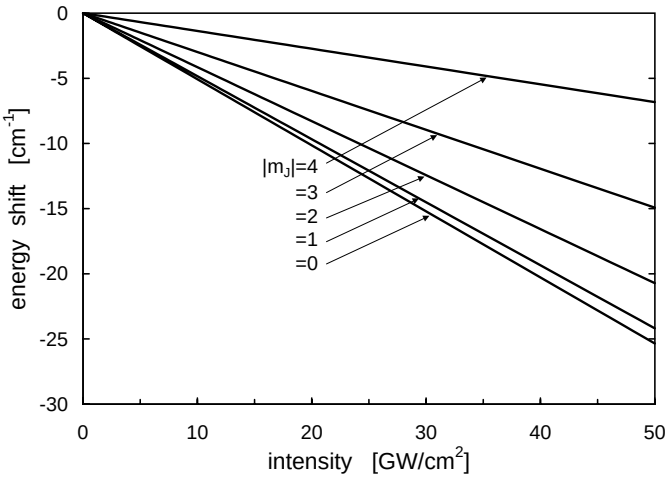

Fig. 1. Stark effect induced energetic splitting of the m_J levels of the $\mathrm{B}\,{}^1\Sigma_u^+$ $(v = 4,\ J = 4)$ state of H_2 as a function of the radiation intensity ($\alpha = 420\times10^{-30}$ m^3, $\gamma = 1\,061\times10^{-30}$ m^3).

Inspecting the theoretical values one notices that both $\alpha_{||}(\omega, R)$ and $\alpha_\perp(\omega, R)$ show strong resonances at the intermolecular distance ($R \approx 1$ Å to 3 Å) and spectral region of interest ($\lambda = 266$ nm and 319 nm). Unfortunately the published data set provides not enough information especially for the R dependence to numerically integrate equation (3) – especially close to the singularities – with sufficient confidence in the result. It is therefore not possible to derive at present accurate effective dynamic polarizabilities $\alpha_{v,||}$ and $\alpha_{v,\perp}$ of the $\mathrm{B}\,{}^1\Sigma_u^+$ state of H_2 from the available theoretical calculations. For the model calculations performed in this paper, however, this theoretical deficiency is without consequence and has no influence on the conclusions. Further, approximate values for the effective polarizabilities are deduced from an experiment, see below.

The energetic shift ΔW of each m_J level due to the quadratic Stark effect is given by [21]

$$\Delta W(m_J) = -\frac{I_{\rm L}}{2c}\left[\alpha - \frac{2}{3}\,\gamma\,\frac{3m_J^2 - J(J+1)}{(2J-1)(2J+3)}\right]. \qquad (4)$$

As an example Figure 1 shows the splitting of the m_J levels of the $\mathrm{B}\,{}^1\Sigma_u^+$ $(v = 4,\ J = 4)$ state of H_2 as a function of the radiation intensity using static polarizabilities. The static isotropic polarizability of this state amounts to $\alpha = 420 \times 10^{-30}$ m^3 and the static anisotropic polarizability to $\gamma = 1\,061 \times 10^{-30}$ m^3 [20]. It is evident that the energetic shift of m_J states with small absolute values are larger than those with a higher value. At an intensity of $I = 10$ GW/cm^2 the $m_J = 0$ level is shifted by about 5.1 cm^{-1} and the $|m_J| = 4$ level by about 1.4 cm^{-1}, causing a splitting of about 3.7 cm^{-1}. Due to the much smaller dynamic polarizabilities of $\alpha \approx 0.8 \times 10^{-30}$ m^3 and of $\gamma \approx 0.3\times10^{-30}$ m^3 [22] of the $\mathrm{X}\,{}^1\Sigma_g^+$ $(v = 0,\ J = 5)$ state in the considered spectral region the Stark induced shifts in the electronic ground state are significantly smaller. At the intensities and spectral line widths discussed here the resulting shifts of this state are negligibly small.

In the following we consider a (1+1′) REMPI detection of linear molecules. The laser field for the resonant transition is assumed to be weak, while the ionizing laser field should saturate the transition. This is a common situation in many REMPI experiments. The ionizing field then induces the AC Stark effect on the rovibronic levels under consideration. Aside a constant factor the ion yield I is then determined by the transition probability for the first resonant excitation step. The relative transition probability between the initial state $|J_\mathrm{i},\, m_\mathrm{i}\rangle$ and the intermediate state $|J_\mathrm{e},\, m_\mathrm{e}\rangle$ is given by:

$$I_\mathrm{Stark}(\chi,\phi) \propto \left|R_\mathrm{e}^{n'n''}\right|^2 |R_{v'v''}|^2 \frac{S_{J'J''}}{2J''+1} \sum_{m_\mathrm{i}'}^{J} N'(J_\mathrm{i}, m_\mathrm{i}') \times \left[f\left(\widetilde{\nu}, \Delta W_\mathrm{i,e}\right) \left|d^{J_\mathrm{e}}_{m_\mathrm{i}' m_\mathrm{S}}(\chi-\phi)\right|^2\right] \left[\begin{pmatrix} J_\mathrm{i} & 1 & J_\mathrm{e} \\ m_\mathrm{i}' & 0 & m_\mathrm{e}' \end{pmatrix}\right]^2 . \quad (5)$$

Here $|R_\mathrm{e}^{n'n''}|^2$ denotes the electronic transition moment, $|R_{v'v''}|^2$ the Franck-Condon-factor, and $S_{J'J''}$ the Hönl-London-factor of the transition. The variables χ and ϕ represent the angles between a space fixed symmetry axis and the polarization directions of the exciting and ionizing laser radiation, respectively. m_S describes the magnetic substates in the system of the ionizing laser radiation. Since this radiation induces the AC Stark effect and thus shifts the energetic position of these states, m_J state population have to be transformed into this coordinate system which is achieved by the rotation matrix $d^J_{m_\mathrm{i} m_\mathrm{S}}, d(\chi-\phi)$ is the well known rotation matrix [23] and describes a coordinate rotation when the polarization of both lasers is not parallel to each other. This allows the treatment of general cases. For parallel polarizations $d^{J_\mathrm{e}}_{m_\mathrm{i}' m_\mathrm{S}}$ reduces to unity, $d^{J_\mathrm{e}}_{m_\mathrm{i}' m_\mathrm{S}} = \delta_{m_\mathrm{i}', m_\mathrm{S}}$. In surface science experiments the surface normal $\widehat{n}$ is often used as quantization axis. For this coordinate system initial states and their population are designated in the following by $|J_\mathrm{i}, m_\mathrm{i}\rangle$ and $N(J_\mathrm{i}, m_\mathrm{i})$, respectively. Since linear polarized radiation is used m_i and m_e are equal. The population of the magnetic substates measured in a coordinate system defined by the polarization direction of the exciting laser is described with $N'(J_\mathrm{i}, m_\mathrm{i}')$, which can be related to the population $N(J_\mathrm{i}, m_\mathrm{i})$ of the space fixed system through the unitary transformation

$$N'(J,m') = \sum_m \left|d^J_{m'm}(\Theta)\right|^2 \langle J,m|\, N(J,m)\, |J,m\rangle\,, \quad (6)$$

where $d^J_{m'm}(\Theta)$ is the well-known rotation matrix [23]. In equation (5) the function f accounts for the spectral dependence of the transition probability,

$$f\left(\widetilde{\nu}, \Delta W_\mathrm{i,e}\right) = \int\!\!\int \frac{I_\mathrm{L}(r,t)}{I_0} \times \exp\left[-\left(\widetilde{\nu} - \widetilde{\nu}_\mathrm{Stark}\left(I(r,t)\right)\right)^2 \frac{4\ln 2}{\Delta\widetilde{\nu}^2}\right] \mathrm{d}r\, \mathrm{d}t. \quad (7)$$

Here $\Delta\widetilde{\nu}$ is the spectral width of the exciting radiation and $\widetilde{\nu}_\mathrm{Stark}\left(I(r,t)\right)$ is the energy shift of a specific level m_S due to the second order Stark effect, which can be calculated for a given laser intensity I_L by equation (4). Since the AC Stark effect affects the energetic position of the individual m_J states differently, an asymmetric spectral line shape results, see below.

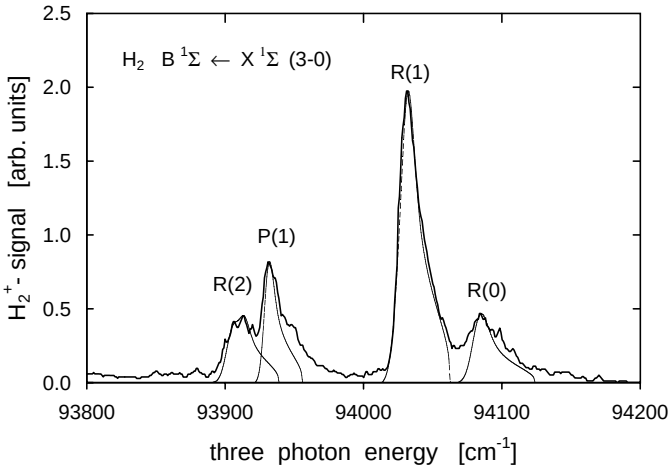

Fig. 2. Experimental (3+1) REMPI spectrum of the $\mathrm{B}\,^1\Sigma_u^+ \leftarrow \mathrm{X}\,^1\Sigma_g^+$ (3–0) band of H_2 of the energy range between 93 800 and 94 200 cm^{-1} [24]. For the simulation a maximum intensity in the Gaussian beam profile of 100 $\mathrm{GW/cm^2}$ and a spectral width of $\Delta\widetilde{\nu} = 0.6\ \mathrm{cm}^{-1}$ of the UV laser field is assumed. The simulation of the four lines in the spectrum are shown as thin lines.

3 Results and discussion

3.1 Line broadening in (3+1) REMPI of H_2

The theoretical considerations are first applied to the simulation of a previously measured (3+1) REMPI spectrum of the $\mathrm{B}\,^1\Sigma_u^+ \leftarrow \mathrm{X}\,^1\Sigma_g^+$ (3–0) Lyman band of hydrogen. This is a typical one-color REMPI experiment, and some implications will be discussed further below. Figure 2 shows this spectrum in the three-photon energy range from 93 800 to 94 200 cm^{-1} ($\lambda = 319.8$ nm to 318.5 nm) [24]. This excitation is three-photon resonant with the $\mathrm{B}\,^1\Sigma_u^+$ ($v = 3$) vibronic state. Tunable laser radiation with a pulse energy of 6 mJ in the UV, a spectral bandwidth of about 0.6 cm^{-1} and a pulse duration of 6 ns (FWHM) was used. This radiation was focused by a lens with a focal length of $f = 80$ mm into a chamber filled with hydrogen ($p(\mathrm{H_2}) = 2\times10^{-7}$ mbar). A measurement of the beam waist showed a radius of $w_0 = 20{-}25\,\mu$m, resulting in a mean intensity at the focus of about 50–80 $\mathrm{GW/cm^2}$. $R(0)$, $R(1)$, $R(2)$, and $P(1)$ rotational lines of this transition can be identified. The spectral width of the $R(1)$ line amounts to about 19 cm^{-1} (FWHM). In addition to the experimental spectrum a simulation of the four lines is shown in Figure 2. The calculation of the line profile followed equation (5), with a Gaussian temporal and spatial variation of the laser intensity. Further, a Gaussian distribution of the pulse-to-pulse fluctuations is assumed

with a variation of ±13% from the maximum intensity at a probability of 50%. At an intensity of $I = 100$ GW/cm^2 in a Gaussian profile a reasonable agreement between the simulation of the line shapes and the experimental line profiles is obtained. Both the theoretically assumed intensity and the experimentally determined one are reasonably close, especially in view of the fact that a smooth experimental intensity profile is assumed which clearly does not describe the real experimental situation. As mentioned above, effective dynamic polarizabilities can not yet be taken from the theoretical considerations. A good agreement of the simulation with the measured spectral lines is obtained for values close to the static polarizabilities ($\alpha = 420 \times 10^{-30}$ m^3 and $\gamma = 1\,061 \times 10^{-30}$ m^3).

3.2 Line broadening in $(1 + 1')$ REMPI

In this section a typical two-color (1+1') REMPI experiment is investigated. In two-color experiments the polarization of the two laser fields involved may be different. Accordingly, four different situations are considered. The linear polarization of both lasers can be both parallel or perpendicular to a space fixed symmetry axis like a surface normal $\hat{n}$, or they can be mutually orthogonal to each other. Of course, also other directions and combinations are possible and can be treated with equation (5). For simplicity, however, we restrict the following discussion to these four most practical situations. The ionization yields obtained are thus distinguished by two indices, the first indicating the polarization direction of the exciting laser with respect to the symmetry axis $\hat{n}$ ($\parallel$ or $\perp$), the second index denotes the polarization direction of the ionizing laser with respect to the same axis $\hat{n}$ ($\parallel$ or $\perp$). In the calculation again a Gaussian temporal and radial laser beam profile is assumed. Since the detection volume is restricted to the Rayleigh length of a focused beam, the intensity is assumed to be constant in the propagation direction. Again the ionizing radiation is chosen to saturate the transition while the exciting radiation is chosen to be weak. This resembles a realistic situation in (VUV + UV) REMPI of hydrogen, nitrogen and other molecules.

3.2.1 Line profile for parallel polarized beams

For calculating the line profile with both laser beams polarized parallel to a space fixed axis $\hat{n}$, $I_{\parallel\parallel}$, first the energetic shift of each m_J rotational level is determined according to equation (4), thereby taking the spatial and temporal variation of the laser intensities into account. In this case both angles χ and ϕ are zero and the rotation matrix $d^{J_e}_{m'm_S}$ reduces to unity, significantly simplifying equation (5). Figure 3a shows for spatial isotropic H_2 the simulated profile of the $P(5)$ line of the $B\,^1\Sigma_u^+ \leftarrow X\,^1\Sigma_g^+$ (4–0) transition at $\lambda = 106.87$ nm for zero detuning. Again, the same values of the dynamic polarizabilities $\alpha_{||}$ and $\alpha_\perp$ for the B state are used as in fitting the experimental (3+1) REMPI spectrum. In this simulation a maximum intensity of the Gaussian beam profile of 10 GW/cm^2 and a spectral width of $\Delta\tilde{\nu} = 1.0$ cm^{-1} of the exciting laser is assumed. The contributions of each m_J state to the total line profile are shown as thin lines. As shown in Figure 1 the amount of the shift depends on the absolute value of m_J and on the laser intensity. The temporal and spatial variation of the beam profile results in the asymmetric spectral line profile for the individual m_J states. Compared to the undisturbed transition the maximum of $|m_J| = 4$ is shifted by -1.1 cm^{-1} and that of $m_J = 0$ by -4.7 cm^{-1}. Since the Stark shift of positive and negative m_J states is degenerated, all states except $m_J = 0$ are considered twice in the summation for the total line profile. Clearly, an asymmetric total line profile is obtained with a maximum intensity at a shift of -4.0 cm^{-1} with respect to the unshifted transition. It should also be noted that for exciting radiation with a narrower spectral width the structures of the profile become more pronounced. Further, in parts of the line profile only a subset of the m_J states are excited.

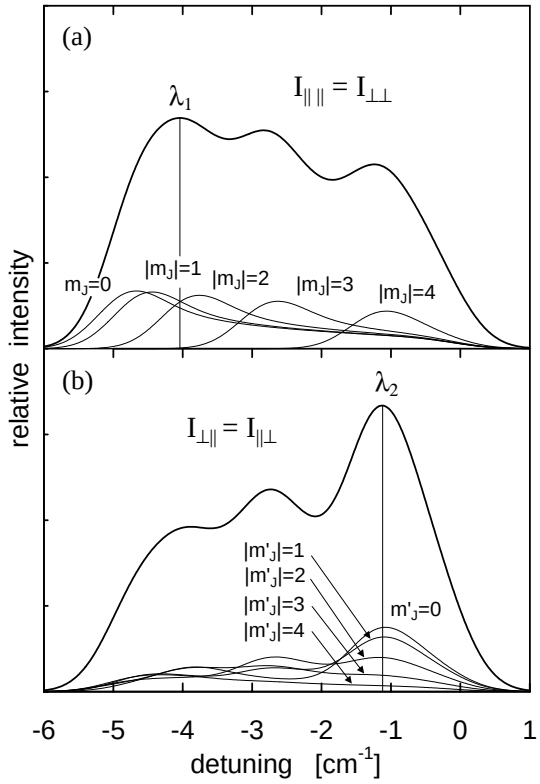

Fig. 3. Simulated profile of the $P(5)$ line of the $B\,^1\Sigma_u^+ \leftarrow X\,^1\Sigma_g^+$ (4–0) transition, shown for spatial isotropic H_2. For the simulation a maximum intensity in the Gaussian beam profile of 10 GW/cm^2 and a spectral width of $\Delta\tilde{\nu} = 1.0$ cm^{-1} of the exciting laser is assumed. The contributions of each m_J state to the line profile are shown as thin lines.

When both lasers are polarized perpendicular to the space fixed axis the rotation matrix $d^{J_e}_{m'm_S}$ in equation (5) again reduces to unity. The population $N(J, m_J)$ has, however, to be transformed to $N'(J, m'_J)$ of the coordinate system rotated by 90°. For spatially isotropically distributed molecules, as assumed in this chapter, the m'_J populations after transformation are identical to the m_J

populations in the coordinate system of the space fixed axis $\widehat{n}$ ($N'(m'_J) = N(m_J)$). Since otherwise the same calculation applies, the line profile for $I_{\perp\,\perp}$ is identical to the line profile for $I_{\parallel\,\parallel}$. It must be emphasized, however, that this only holds for isotropically distributed molecules.

3.2.2 Line profile for perpendicular polarized beams

For perpendicular polarization of both laser fields the enclosed angle is $(\chi - \phi) = 90°$ and thus in equation (5) the rotation matrix d has properly to be taken into account. For $I_{\perp\,\parallel}$ the state selective excitation step occurs in the unprimed coordinate system. The Stark field, however, acts on m_J populations which first have to be transformed from the primed to the unprimed coordinate system. Since this transformation projects m_J states to all m'_J states, the individual line profile of the m'_J states are thus shifted and broadened to a similar extent. Figure 3b shows the line profiles for this configuration using the same intensities and beam profiles as before. It is evident that all profiles of the individual m'_J states are now broadened over the whole profile, different from Figure 3a. The total line profile is now at maximum shifted by $-1.1\,\mathrm{cm}^{-1}$ with respect to the undisturbed transition, and its position is different from that of the $I_{\parallel\,\parallel}$ configuration. When the transition is probed by a laser with a spectral width narrower than the broadening of the profile, all m'_J states are probed, albeit to a different extent at different positions within the profile. This again has a significant influence on the determination of a rotational alignment by changing the polarization of the exciting laser field.

3.3 Detection of alignment information

The above simulations have shown that under the influence of the Stark effect the spectral lines connecting appropriate m_J states are shifted and broadened, however, to a different extend for $I_{\parallel\,\parallel}$ and $I_{\perp\,\parallel}$ situations. In this section we will calculate the quadrupole alignment for a specific case to demonstrate the influence of the second order AC Stark effect. The molecular constants used are again those for the $\mathrm{B}\,^1\Sigma_u^+ \leftarrow \mathrm{X}\,^1\Sigma_g^+$ (4–0) Lyman transition of hydrogen. Since for the $\mathrm{X}\,^1\Sigma_g^+$ ground state the polarizabilities α and γ are smaller by about three orders of magnitude than for the B state, level shifts and splittings are predominantly caused by the influence of the Stark effect on the B state. The extend of the information deterioration depends not only on the laser intensity but also on the spectral width of the exciting radiation relative to the broadened line profile. An inspection of Figure 1 shows that the spectral widths of modern tunable lasers may be significantly narrower than levels shifts and splittings in the focus of the beam. To generalize the analysis we introduce a splitting parameter $S = I_\mathrm{L}/\Delta\widetilde{\nu}_\mathrm{L}$, where the intensity of the Stark radiation is divided by the spectral width $\Delta\widetilde{\nu}_\mathrm{L}$ of the exciting laser radiation.

For the simulation it is assumed that the measurements are generally conducted at the maximum of the spectral line. The spectral position of this line maximum depends on the choice of the relative polarizations of the exciting and ionizing laser, as shown in Figure 3. For parallel polarization of both radiations the maximum ion signal occurs in spatially isotropic H_2 at the wavelength λ_1 as indicated in Figure 3a. When both lasers are polarized perpendicular to each other the maximum ion yield is observed at λ_2 (Fig. 3b). λ_1 is shifted further away from the undisturbed transition than λ_2. The positions of both wavelengths depend of course on the intensity of the Stark broadening laser radiation. Beside measurements at these two different wavelengths also two different methods for the measurement of the anisotropy P are considered. In the illustrations below the index "fix" denotes a determination of the anisotropy with the polarization of the ionizing laser directed always parallel to the space fixed symmetry axis $\hat{n}$, while the polarization of the exciting laser is varied from parallel to perpendicular to $\hat{n}$. The index "var" indicates that the polarization of the ionizing laser as well as that of the exciting laser is varied with respect to $\hat{n}$, but both being always parallel to each other. Similarly, different anisotropies P are defined depending on the relative polarizations of both lasers

$$P_\mathrm{fix} = \frac{I_{\parallel\,\parallel} - I_{\perp\,\parallel}}{I_{\parallel\,\parallel} + I_{\perp\,\parallel}} \tag{8}$$

and

$$P_\mathrm{var} = \frac{I_{\parallel\,\parallel} - I_{\perp\,\perp}}{I_{\parallel\,\parallel} + I_{\perp\,\perp}}. \tag{9}$$

Both are determined at the two wavelengths λ_1 and λ_2. From the anisotropy P the quadrupole alignment factor $A_0^{(2)}$ may be derived [25], which yields for R-branch excitation

$$A_0^{(2)} = \frac{-4\,(2J_i + 3)}{J_i\,(3 - P)}\,P\,, \tag{10}$$

and for the P-branch excitation

$$A_0^{(2)} = \frac{-4\,(2J_i - 1)}{(J_i + 1)\,(3 - P)}\,P. \tag{11}$$

In the simulation the anisotropy P is calculated from the contribution of each m_J state to the ion intensity at the wavelengths λ_1 and λ_2. Thus four different situations are distinguished and indicated with $A_0^{(2)}(\lambda_1, \mathrm{fix})$, $A_0^{(2)}(\lambda_1, \mathrm{var})$, $A_0^{(2)}(\lambda_2, \mathrm{fix})$ and $A_0^{(2)}(\lambda_2, \mathrm{var})$.

3.3.1 Isotropic ensemble

In Figure 4 the alignment parameter $A_0^{(2)}$ derived in this way is shown for spatially isotropic hydrogen molecules. The splitting parameter S or the respective intensity at a spectral width of $1\,\mathrm{cm}^{-1}$ is varied from 0.1 to $100\,\mathrm{GW\,cm^{-2}/cm^{-1}}$. Two different results can be noticed for the two situations where the polarization of the intense

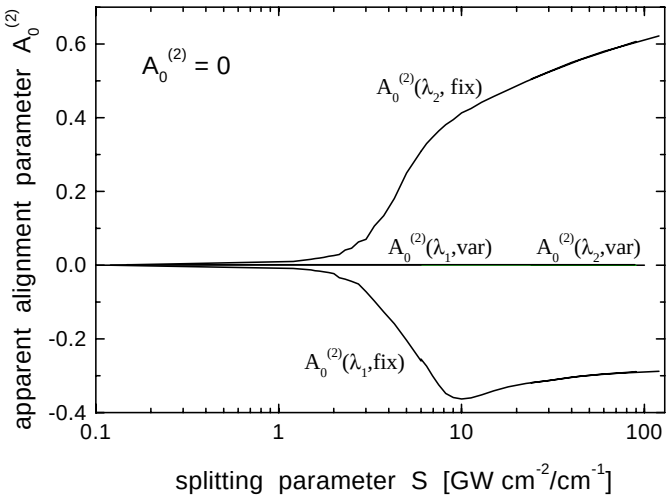

Fig. 4. Apparent alignment parameter $A_0^{(2)}$ for spatially isotropic H_2. The different measurement situations are described in the text.

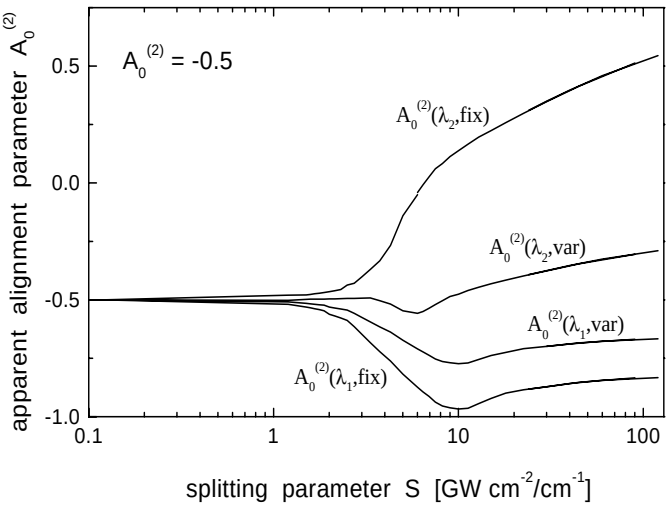

Fig. 5. Apparent alignment parameter $A_0^{(2)}$ for cartwheeling molecules with a true $A_0^{(2)} = -0.5$.

ionizing laser is either fixed or variable. When the polarization of the ionizing laser is rotated together with that of the exciting laser $(A_0^{(2)}, \text{var})$ the deduced alignment is always zero at both wavelengths λ_1 and λ_2, as expected for an isotropic distribution. The reason for this behaviour is the identical influence of the Stark effect on the intensities $I_{\parallel\parallel}$ and $I_{\perp\perp}$, which can be noticed in Figure 3a. Therefore the signal difference between both intensities is always zero, and an anisotropy $P = 0$ corresponds to an alignment factor of $A_0^{(2)} = 0$. At a first glance this insensitivity of the result on the splitting parameter S or the laser intensity makes this measurement geometry ideally suited for REMPI determinations of an alignment. However, this insensitivity does not hold for an anisotropic ensemble, as we will shown below. This phenomenon makes it on the other hand impossible to test with an isotropic gas phase ensemble a possible influence of the Stark effect on an alignment result for a specific experimental arrangement. This may be especially important for one-color REMPI, where the polarizations of both laser fields are identical.

For the other measurement situation where the polarization of the Stark laser is fixed parallel to the space-fixed axis $\hat{n}$ a strong dependence of the apparent alignment on the laser intensity or the splitting parameter can be noticed. Up to an intensity of 1 GW/cm^2 and a spectral width of the exciting laser of 1 cm^{-1} or larger the influence of the Stark effect can be neglected. For higher intensities or a narrower spectral width, however, a significant falsification of the real alignment occurs. For example at $S = 10$ GW cm^{-2}/cm^{-1} one deduces an apparent alignment of $A_0^{(2)} = -0.36$ at λ_1 and $A_0^{(2)} = 0.41$ at λ_2. In the former case the molecules seem to be strongly cartwheeling, in the latter case strongly helicoptering, while in fact the ensemble is isotropically distributed. This apparent molecular alignment results if for the determination of the alignment factor an undisturbed system is assumed, but the Stark effect significantly influences the measurement.

3.3.2 Aligned molecules

When the molecular ensemble is partially aligned the situation becomes worse. Again we simulate apparent alignment parameters $A_0^{(2)}$ for the $P(5)$ line of the $B\,^1\Sigma_u^+ \leftarrow X\,^1\Sigma_g^+$ (4–0) Lyman transition in hydrogen. Assuming first a negative alignment with $A_0^{(2)} = -0.5$, thus a cartwheeling motion of the molecules with respect to the space fixed axis $\hat{n}$. Higher moments are set to zero for simplicity. The populations of the m_J levels are thus described by a pure parabolic function with the highest population in $m_J = 0$. Figure 5 shows the apparent alignment parameter $A_0^{(2)}$ obtained for this case as a function of the splitting parameter. As for the spatially isotropic ensemble up to the intensity of 1 GW/cm^2/cm^{-1} spectral intensity the real alignment is not affected by the Stark effect. At higher intensities again a significant change of the apparent alignment parameter compared to the real value occurs. Now both geometries with a space-fixed and a variable polarization of the Stark effect inducing laser are affected, although the influence on $A_0^{(2)}$ is much more significant for the space-fixed polarization.

Assuming a positive alignment of the molecular ensemble of $A_0^{(2)} = +0.5$, thus molecules with a helicoptering motion, yields in effect similar results, as shown in Figure 6. Again up to 1 GW/cm^2/cm^{-1} the determination of the alignment is not affected by Stark shifts of the m_J states. At higher intensities an influence can again be noticed. In this case, however, the influence is larger for the situation where the polarization of both the exciting and the strong Stark laser field are varied together. When the polarization of the Stark laser is kept fixed and parallel to the space-fixed axis $\hat{n}$ the apparent alignment assumes at

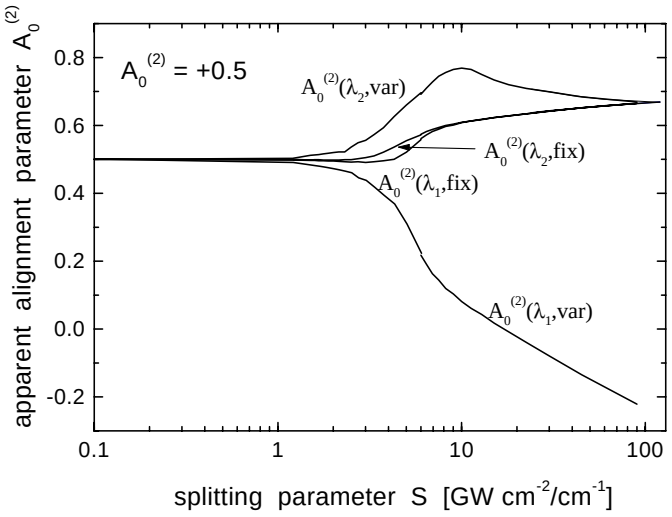

Fig. 6. Apparent alignment parameter $A_0^{(2)}$ for helicoptering molecules with a true $A_0^{(2)} = +0.5$.

most (at 100 GW cm^{-2}/cm^{-1}) a value of $A_0^{(2)} = +0.65$, slightly higher than the real value. In realistic measurement situations this often remains within the margin of error for the deduced quadrupole alignment. This comparatively insensitive function of $A_0^{(2)}$ on the Stark shift is caused by the fact that for a positive alignment the higher m_J states which experience in the present example a weaker Stark shift, are preferentially populated.

4 Conclusions

In conclusion we have shown that the second order Stark effect significantly influences the alignment parameter $A_0^{(2)}$ derived for aligned ensembles. For polarizabilities of $\gamma \geq 10^{-27}\,\mathrm{m}^3$ and $\alpha \geq 10^{-28}\,\mathrm{m}^3$ the Stark effect becomes significant at splitting parameters higher than $S = 1$ GW cm^{-2}/cm^{-1}. With this values of α and γ the asymmetric broadening of the H_2 spectral lines in the $B\,^1\Sigma_u^+ \leftarrow X\,^1\Sigma_g^+$ (3–0) Lyman transition observed in a (3+1) REMPI experiment can well be described. At lower values of this parameter S the Stark induced energetic shifts of the m_J levels are smaller than the spectral width of the exciting radiation. The intensities up to which no influence occurs depend of course on the value of γ, the anisotropic polarizability. It should also be noted that the true alignment value can always be obtained when in equations (8) and (9) the integral of the spectral lines $I_{\parallel\parallel}$ and $I_{\perp\parallel}$ are taken, when thus the exciting laser is scanned over the line profile. In two recent experiments the alignment of D_2 molecules associatively desorbing from Pd(100) and Cu(111) surfaces has been measured *via* the $B\,^1\Sigma_u^+ \leftarrow X\,^1\Sigma_g^+$ transition by laser induced fluorescence (LIF) [8,26] and by (1+1′) REMPI [7]. In the latter experiment the splitting parameter amounted to 100 MW cm^{-2}/cm^{-1} [7], thus well below the critical value of 1 GW cm^{-2}/cm^{-1}. It may be interesting to note that both the LIF and the REMPI measurement yielded for the quadrupole alignment at different J within the statistical error the same results.

In general the model calculations demonstrate that one must be careful in interpreting alignment data obtained by REMPI experiments. When the applied intensity exceeds a limit given by the spectral width of the lasers and the specific dynamic polarizabilities α and γ, the observed line profiles will be asymmetricly broadened or distorted. In that case only a subset of directional substates m_J can be detected by the experiment and the transition probability will depend on the quantum number of the substate. Analyzing such experimental data with the aim to obtain information on the alignment parameter A_0^k requires a detailed knowledge about the dynamic polarizabilities. It is also obvious that detailed theoretical calculations of such dynamic polarizabilities for electronically excited molecules are highly desirable for the interpretation of AC Stark broadened lines. In cases where the intermediate level is resonantly coupled by strong fields to other states coherence effects not considered here will considerably hamper the determination of a rotational angular momentum alignment already at lower intensities.

The authors wish to thank J. Rychlewski for discussion and for providing unpublished data of the dynamic polarizabilities. Financial support by a grant from the Deutsche Forschungsgemeinschaft (Za 110/15-2 and 17-2) is gratefully acknowledged.

References

1. C.H. Greene, R.N. Zare, J. Chem. Phys. **78**, 6741 (1983).
2. A.C. Luntz, A.W. Kleyn, D.J. Auerbach, Phys. Rev. B **25**, 4273 (1982).
3. A.W. Kleyn, A.C. Luntz, D.J. Auerbach, Surf. Sci. **117**, 33 (1982); Surf. Sci. **152/153**, 99 (1985).
4. A.C. Kummel, G.O. Sitz, R.N. Zare, J.C. Tully, J. Chem. Phys. **89**, 6947 (1988).
5. D.C. Jacobs, R.J. Madix, R.N. Zare, J. Chem. Phys. **85**, 5469 (1986).
6. I. Beauport, K. Al-Shamery, H.-J. Freund, Chem. Phys. Lett. **256**, 641 (1996).
7. S.J. Gulding, A.M. Wodtke, H. Hou, C.T. Rettner, H.A. Michelsen, D.J. Auerbach, J. Chem. Phys. **105**, 9702 (1996).
8. D. Wetzig, R. Dopheide, M. Rutkowski, R. David, H. Zacharias, Phys. Rev. Lett. **76**, 463 (1996).
9. B. Girard, N. Billy, J. Vigué, J.C. Lehmann, Chem. Phys. Lett. **102**, 168 (1983).
10. W.M. Huo, K.P. Gross, R.L. McKenzie, Phys. Rev. Lett. **54**, 1012 (1985).
11. D.C. Jacobs, R.N. Zare, J. Chem. Phys. **85**, 5457 (1986).
12. B. Girard, G.O. Sitz, R.N. Zare, N. Billy, J. Vigué, J. Chem. Phys. **97**, 26 (1992).
13. A.D. Rudert, J. Martin, H. Zacharias, J.B. Halpern, Chem. Phys. Lett. **294**, 381 (1998).
14. J. Vigué, P. Grangier, G. Roger, A. Aspect, J. Phys. France **42**, L531 (1981).
15. R. Neuhauser, H.J. Neusser, J. Chem. Phys. **103**, 5362 (1995).

16. R. Neuhauser, R. Sussmann, H.J. Neusser, Phys. Rev. Lett. **74**, 3141 (1995).
17. S. Schiemann, A. Kuhn, S. Steuerwald, K. Bergmann, Phys. Rev. Lett. **71**, 3637 (1993).
18. A.R. Edmonds, *Angular Momentum in Quantum Mechanics* (Princeton University Press, Princeton, 1960).
19. A. Messiah, *Quantum Mechanics* (North-Holland, Amsterdam, 1962).
20. J. Rychlewski, J. Komasa, W. Cencek, Phys. Rev. A **41**, 5825 (1990).
21. H. Moosmüller, C.Y. She, W.M. Huo, Phys. Rev. A **40**, 6983 (1989).
22. D.M. Bishop, L.M. Cheung, J. Chem. Phys. **72,** 5125 (1980).
23. R.N. Zare, *Angular Momentum* (Wiley-Interscience, New York, 1988).
24. W. Meier, Ph.D. thesis, University of Bielefeld, 1986.
25. C.H. Greene, R.N. Zare, Annu. Rev. Phys. Chem. **33**, 119 (1982).
26. D. Wetzig, M. Rutkowski, R. David, H. Zacharias, Europhys. Lett. **36**, 31 (1996).